JGR Space Physics

RESEARCH ARTICLE
10.1029/2019JA027372

Understanding and Harnessing the Dual Electrostatic/Electromagnetic Character of Plasma Turbulence in the Near-Earth Space Environment

Gurudas Ganguli[1], Chris Crabtree[1], Alex C. Fletcher[1], Leonid Rudakov[2], Andrew S. Richardson[1], Joseph Huba[3], Carl Siefring[1], William Amatucci[1], and Charlton D. Lewis[4]

[1]Plasma Physics Division, Naval Research Laboratory, Washington, DC, USA, [2]Trinum Research, San Diego, CA, USA, [3]Syntek Technologies, Fairfax, VA, USA, [4]Air Force Institute of Technology, Wright-Patterson AFB, OH, USA

Key Points:
- SMART is an active experiment to study the evolution of turbulence in the natural plasma environment
- Fast neutral barium beam injection in ionosphere will produce lower hybrid waves to pump turbulence
- Nonlinear conversion of lower hybrid to whistler waves and escape to radiation belts to be monitored

Correspondence to:
G. Ganguli,
guru.ganguli@nrl.navy.mil

Citation:
Ganguli, G., Crabtree, C. E., Fletcher, A. C., Rudakov, L., Richardson, A. S., Huba, J., et al. (2019). Understanding and harnessing the dual electrostatic/electromagnetic character of plasma turbulence in the near-earth space environment. *Journal of Geophysical Research: Space Physics*, *124*, 10,365–10,375. https://doi.org/10.1029/2019JA027372

Received 17 SEP 2019
Accepted 14 NOV 2019
Accepted article online 21 NOV 2019
Published online 03 DEC 2019

Abstract The ability to morph electrostatic plasma turbulence into electromagnetic has promising applications, including the possibility of actively influencing the near-Earth plasma state, aka the space weather. This dual (electrostatic/electromagnetic) nature is a fundamental property of plasma turbulence, which has not been well explored but could explain many phenomena including the formation of a resonant cavity that can amplify the turbulence energy. The upcoming Space Measurement of A Rocket-Released Turbulence (SMART) mission is designed to understand the evolution of plasma turbulence and the nonlocal consequences of its dual nature. This includes the flow of energy into all possible wavelengths, as well as the transport of energy over a large geographical volume. The resulting energy redistribution in both waves and particles in an extended geographical volume creates a unique electromagnetic environment, which is important for space weather.

1. Introduction

Magnetized plasmas display a much larger degree of freedom than neutral fluids in terms of oscillations that a medium can support. The ability of plasma waves to interchange between electrostatic and electromagnetic character has unique consequences. This makes the evolution of turbulence in plasmas considerably more complex than in neutral fluids. In plasmas the magnetic field breaks the symmetry and introduces a specific direction making the wave vector spectrum anisotropic. Consequently, the frequency of oscillations in a plasma medium is not always directly proportional to the wave vector as is the case in a neutral medium. The existence of collisionless dissipation in plasma, that is, Landau and cyclotron damping, allows for kinetic interactions between waves and plasma particles through Landau and cyclotron resonances. This can substantially affect the evolution of turbulence, giving rise to a spectrum far from the Kolmogorov $k^{-5/3}$ power law (Kolmogorov, 1941) that characterizes turbulence in neutral media (here k is the magnitude of the wave vectors of the turbulent fluctuations). A major implication is that the flow of energy in magnetized plasma is not necessarily Kolmogorov-like, with a local cascade of energy to shorter length scales. Nonlinear kinetic interactions in plasma turbulence allow for nonlocal flow of energy to longer length scales as well as to larger geographical volumes (Ganguli et al., 2010). Hence, the saturation process in plasma turbulence can result in a variety of final plasma states. Besides academic interest, this also has practical implications, particularly in space because the dynamics of plasma turbulence can affect space weather.

Extreme space weather that occurs during periods of high solar activity can be hazardous to space assets, which are indispensable to our society today. One such hazard is the enhancement of flux in the radiation belts, which are formed by energetic electrons trapped in the Earth's dipolar magnetic field (Schulz & Lanzerotti, 1974; Van Allen et al., 1959). An outstanding question in near-Earth space weather is why some geomagnetic storms produce enhanced radiation belts and why some show depletion or remain unchanged (Reeves et al., 2003). Understanding and forecasting such space weather events, and to some extent actively influencing the return to normalcy from extreme conditions, have become a societal necessity. For accomplishing this, a deeper understanding of the dynamics of near-Earth space weather is necessary, but such understanding is predicated upon the knowledge of the evolution of turbulence and transport of energy and

momentum in unbounded magnetized plasma. Therefore, the objective of the upcoming Space Measurement of A Rocket-Released Turbulence (SMART) mission is to use the ionosphere as an outdoor laboratory to study the behavior of plasma turbulence in the actual environment of interest. The SMART mission is designed and executed by the U.S. Naval Research Laboratory and sponsored by the Defense Advanced Research Projects Agency.

Study of plasma turbulence has been largely motivated by in situ observations in space. For large magneto-hydrodynamic scales, the evolution of plasma turbulence is generally found to be Alfvenic with dispersion relation $\omega = kV_A$, where $V_A = B/\sqrt{4\pi n m_i}$ is the Alfven velocity and n and m_i are density and ion mass, respectively, and ω is the frequency (Sorriso-Valvo et al., 2007). Since $\omega \propto k$, the spectral character is largely similar to a neutral medium with power varying closely as $\sim k^{-5/3}$ (Sorriso-Valvo et al., 2007), although there is no physical reason why magnetized plasma should behave as a neutral fluid. In this regime the turbulence is characterized by a single time scale with $\omega\tau \sim 1$ (i.e., $\omega \sim \gamma \sim kV$, where γ is the imaginary part of the frequency) and spatially forms a self-organized nonlinear structure. This is defined as the strong turbulence regime. Collisionless wave-particle interactions do not play a major role in strong turbulence. This changes as the length scale reduces toward the ion inertial length, where a distinct spectral break appears (Alexandrova et al., 2009), indicating a change in the underlying physics. A similar spectral break has recently been observed in a laboratory experiment as well (Chatterjee et al., 2017). We argue that, for short scales around the ion inertial length or below, a variety of multi-scale linear, nonlinear, and kinetic processes come into play that can affect the turbulent oscillations and dispersive properties in the medium (Rudakov et al., 2011; Rudakov, Crabtree, Ganguli, et al., 2012). This results in an ensemble of waves with $\omega\tau \gg 1$, with uncorrelated phases and for which particle dynamics are important. These waves may include linear growth or damping as well as nonlinear processes—such as induced scattering, decay, and coalescence—and have time scales τ much longer than the wave period $1/\omega$. Collectively, this phenomenon is defined as weak turbulence and is the next step from quasi-linear evolution in the hierarchy of plasma dynamics. Weak turbulence is commonplace in the Earth's immediate neighborhood, and hence, its relationship to the near-Earth space weather is an obvious fundamental science issue, which is still largely outstanding.

Accurate characterization of turbulence in space is challenging because observations pertain to the saturated state while the initial conditions are unknown. This introduces ambiguities as it is difficult to separate the cause from the effect. Laboratory reproduction of space turbulence is also difficult because the wave vector spectrum is limited by quantization effects in a finite-size device. In addition, it is often difficult to scale the background parameters and the realistic field geometry accurately in the laboratory. Therefore, the SMART experiment is designed to be carried out in the ionosphere itself. Broadband waves in the intermediate frequency range, $\Omega_i < \omega < \Omega_e$ (where $\Omega_{i,e}$ are ion and electron gyrofrequencies) will be introduced into the ionosphere by injecting a high-speed beam of neutral barium atoms from a sounding rocket. The kinetic energy of these photo-ionized barium atoms will seed electrostatic waves and induce weak turbulence. This will provide a complete knowledge of the initial condition of the turbulence. The evolution of the turbulence will be monitored through measurements of the intermediate stages until saturation. With the knowledge of initial, intermediate, and final states, a holistic picture of the turbulent evolution of the plasma and its effects in the space environment will emerge.

2. SMART Experiment Description

Figure 1 schematically describes the SMART experiment. The SMART mission is modeled after similar experiments conducted since the mid-1970s generating a high-speed Barium (Ba) release by a shaped charge explosion to accelerate the Ba atoms to high velocities perpendicular to the Earth's magnetic field (Koons & Pongratz, 1981). The Ba atoms photo-ionize, forming a ring velocity distribution of heavy Ba+ ions that is unstable to lower hybrid waves (Mithaiwala et al., 2010).

The sounding rocket will carry the Ba release module and an instrumented daughter section that includes vector wave magnetic and electric field sensors, Langmuir probes, and plasma resonance probes. The goal of these measurements is to determine the whistler/magnetosonic and lower hybrid wave amplitudes, spectra, and characterize the initial ionospheric conditions in the source region. In contrast with previous experiments, the SMART instrument payload will be able to measure both electrostatic and electromagnetic waves. We expect wave frequencies of 5–10 kHz and electrostatic wave amplitudes of approximately 350 mV/m.

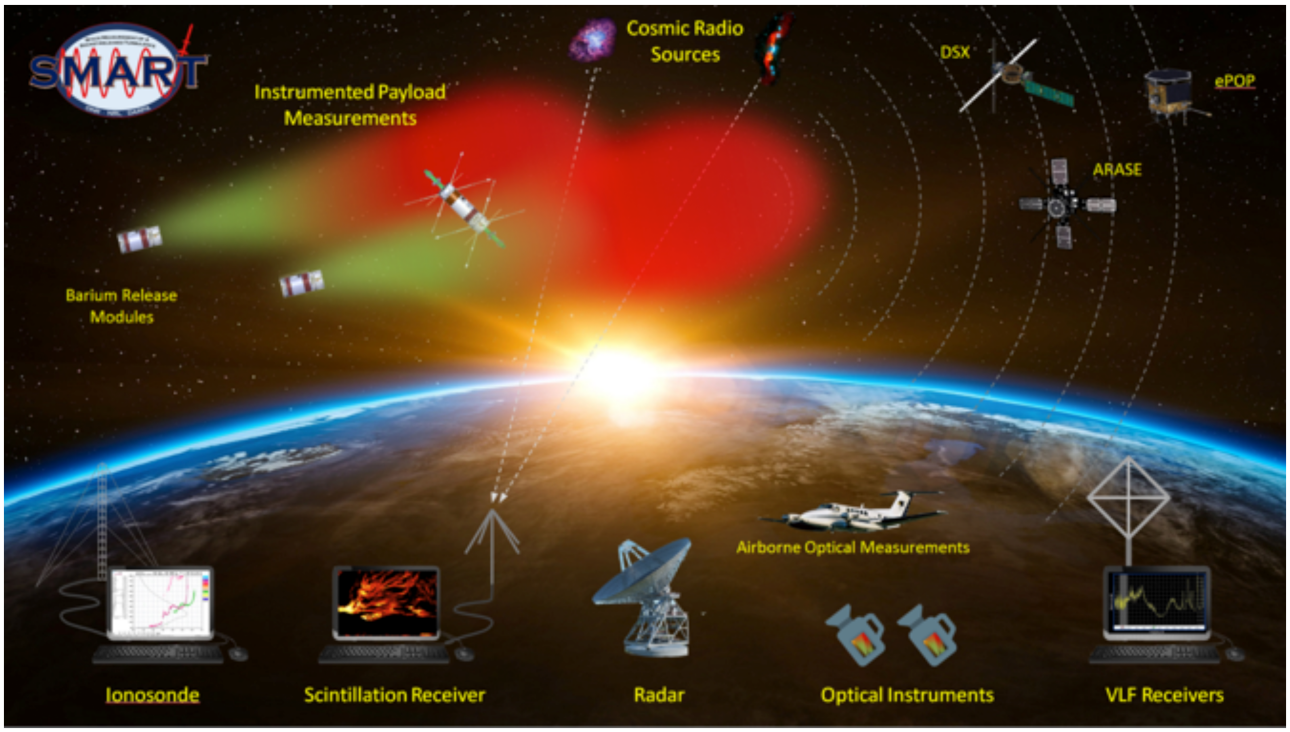

Figure 1. A schematic sketch for the SMART Ba release experiment. A mother-daughter sounding rocket is launched when one or more satellites are in a proper location to observe whistler in the inner magnetosphere. The Ba release module separates from an instrumented section and injects the high-speed Ba perpendicular to the Earth's magnetic field. The Ba/Ba+ cloud envelopes the instrumented payload. Comprehensive wave measurements are made both in the ionosphere and magnetosphere. An assortment of ground-based diagnostics are used to characterize the Ba release, ionization, structuring, and the background ionospheric conditions.

The expected wavelengths depend strongly on propagation angle and will be on the order of meters for electrostatic waves and approximately 10 km for electromagnetic waves.

The Ba release will occur at 550 km near apogee. Figure 1 additionally shows a second release from a second sounding rocket, which would occur about 15 s after the first. The purpose is to increase the energy density of the waves in order to enhance the nonlinear scattering rate. The scattering rate is proportional to the square of the wave field amplitude (equation (3)); the waves from the second release will experience a larger scattering rate from the magnetospheric end. In addition, the waves from the second release will confirm the results from the first, thereby positively ruling out any natural source for the waves. Ground-based cameras and radio diagnostics will be used to characterize the Ba release. One or more satellites in the magnetosphere, for example, the Japanese Arase/ERG, the Air Force DSX, or the Canadian Cassiope/ePOP, can be used to detect the propagation of the SMART-generated whistler/magnetosonic waves into the radiation belts.

3. The Fate of the Energy

To anticipate the outcome of the SMART experiment we follow the energy in the beam of transversely injected neutral Ba atoms. This energy is extracted from the beam by the generation of electrostatic waves that evolve nonlinearly into electromagnetic waves, which then radiate into the magnetosphere. After photo-ionization, the Ba+ ions are confined by the magnetic field to form a ring velocity distribution as shown in a test particle simulation in Figure 2. In this simulation, neutral Barium particles were released according to a distribution from Koons and Pongratz (1981) that includes a drifting Maxwellian moving at 9.4 km/s and a non-drifting Maxwellian; the drifting population contains significantly fewer particles than the non-drifting population. The Barium neutrals are allowed to randomly photo-ionize with a photo-ionization time scale of 30 s. Figures 2a and 2b show the fast Ba+ density 10 s after release obtained from the test particle simulation. The distribution in Figure 2c is at a point along the axis 9.4 km from the release point, which is near the expected trajectory of the SMART instrument payload. This distribution is

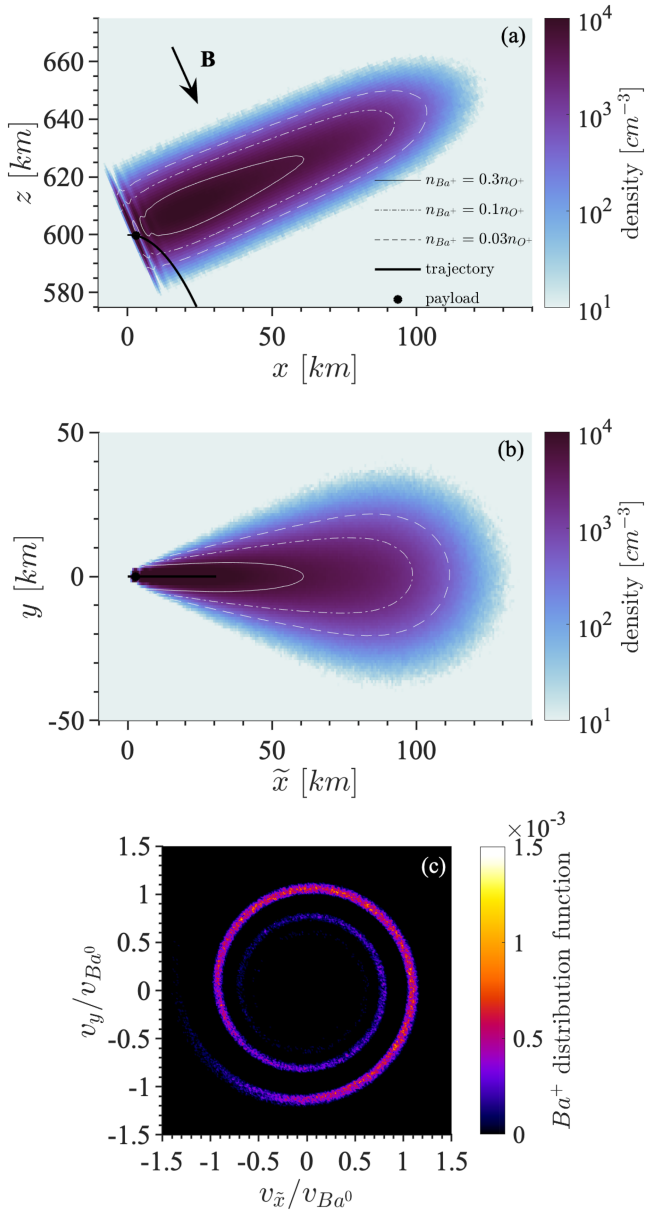

Figure 2. A test particle simulation of the expansion and ionization of the fast barium population. The density in a cut along a central plane parallel to the magnetic field is shown in (a), along with the magnetic field direction and trajectory of the instrument payload. The density in a cut along a central plane perpendicular to the magnetic field is shown in (b). Both (a) and (b) are 10 s after release. Panel (c) shows the distribution function at a point 9.4 km from the release point 2 s after release. This anisotropic and non-gyrotropic helical distribution is expected to be observed by the instrument payload.

far from thermodynamic equilibrium. Consequently, in the collisionless ionosphere, it will relax toward a stable Maxwellian distribution through the emission of waves.

Among the waves that appear at the earliest time—and which then induce plasma turbulence—are the lower hybrid waves with a growth rate (Mithaiwala et al., 2010) of

$$\gamma_r = \omega\alpha^{2/5}\frac{\sin(4\pi/5)}{2}, \tag{1}$$

where $\alpha \equiv (n_{Ba}/n_i)(m_i/m_{Ba})$ and m_s denotes the mass of species s. Figure 3 shows the results of a particle-in-cell (PIC) simulation of these waves in the ionospheric conditions that will be encountered in the

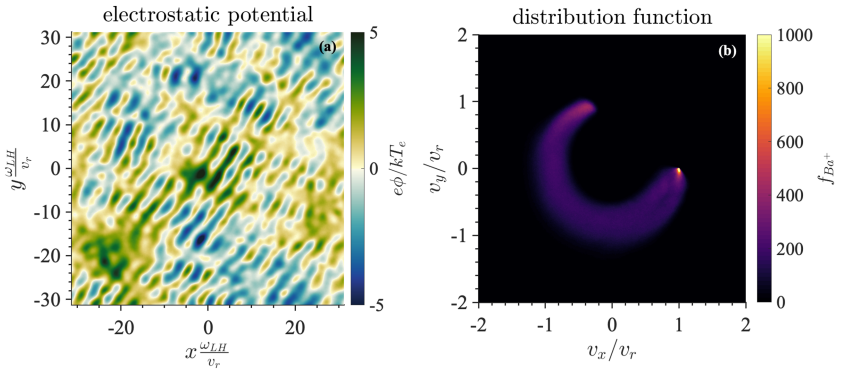

Figure 3. A particle-in-cell simulation of a ring forming with finite-time photo-ionization, becoming unstable, and exciting lower hybrid waves. The resulting electrostatic waves are seen in the potential (a); note that there is a preferred direction for the wave vector due to the anisotropy in the distribution function. The velocity distribution function of a partial ring is shown in (b). In (b), there is a constant source of new barium ions at $(v_x, v_y) = (v_r, 0)$.

SMART experiment. The PIC simulation is 2D electrostatic with streaming neutrals ionizing with a characteristic time scale of three times the cyclotron period, which is also much longer than the growth rate of the waves. This simulation uses parameters similar to those in Winske and Daughton (2012). There are four species: electrons, background ions (oxygen), ring ions (barium), and beam neutrals (barium). The electron to background ion mass ratio is $m_i/m_e = 500$, and the ring ion to background ion mass ratio is $m_r/m_i = 4$. The fraction of beam neutrals (which become ring ions) to total ions is 0.3, and the simulation takes place in the perpendicular plane with $B = 1/\sqrt{3}$. The electron plasma frequency is $\omega_{p,e} = 1$, the electron thermal speed is $v_{t,e} = \sqrt{0.001}$, and the beam speed is $v_r = 7v_{t,i}$, where $v_{t,i}$ is the background ion thermal speed. The electrostatic potential and resulting waves are shown in Figure 3a, while the formation of the ring and velocity space diffusion from the instability is shown in Figure 3b. The wave frequency is around the local lower hybrid frequency. Further details on the PIC simulations with photo-ionization are provided in an upcoming manuscript.

For the parameters of the SMART experiment, the order of magnitude growth rate of the lower hybrid waves is $\gamma_r \sim 10^3/s$ (Ganguli et al., 2015). These waves are a branch in the family of intermediate frequency waves with electromagnetic dispersion relation in cold plasma given approximately by (Ganguli et al., 2010)

$$\frac{\omega^2}{\Omega_e^2} = \left[\mu + \frac{\bar{k}_\parallel^2}{1+\bar{k}_\perp^2}\right]\frac{\bar{k}^2}{1+\bar{k}^2}, \tag{2}$$

where $\mu = m_e/m_i$ is the ratio of electron to ion mass, $\bar{k} = kc/\omega_{pe}$ is the wave vector normalized by electron skin depth, $\bar{k}_\perp^2 = \bar{k}_x^2 + \bar{k}_y^2$, $k_z \equiv k_\parallel$, $\bar{k}^2 = \bar{k}_\perp^2 + \bar{k}_\parallel^2$, c is the speed of light, $\omega_{pe} = \sqrt{4\pi n_e e^2/m_e}$ is the electron plasma frequency (with e and n_e representing electron charge and density respectively), and $\parallel$ and $\perp$ refer to the directions parallel and perpendicular to the magnetic field which is assumed in the z direction. The lower hybrid frequency is $\omega_{LH} \approx \sqrt{\Omega_i\Omega_e}$ in the dense ionospheric plasma where $\omega_{pe} > \Omega_e$. For $\bar{k}_\parallel^2 > \mu$ and $\bar{k}_\perp^2 < 1$, the dispersion relation given by equation (2) reduces to the electromagnetic whistler wave dispersion relation. For $1 > k_\parallel^2/k_\perp^2 > \mu$ and $\bar{k}_\perp^2 > 1$, it reduces to the dispersion relation of what are sometimes referred to as electrostatic whistler waves. For $k_\parallel^2/k_\perp^2 < \mu$ and $\bar{k}_\perp^2 > 1$, it reduces to the dispersion relation of electrostatic lower hybrid waves. For $\bar{k}_\parallel^2 < \mu$ and $\bar{k}_\perp^2 < 1$, it reduces to the dispersion relation for electromagnetic magnetosonic waves.

Thus, both whistler and lower hybrid waves belong to the same family of intermediate frequency range waves, and they can morph into each other seamlessly as a function of the wavelength. This is unlike the mode conversion process in which two distinct modes exist for exactly the same parameters. Instead, for shorter wavelengths ($\bar{k}_\perp > 1, k_\perp > k_\parallel$), the electrostatic character of these waves becomes prominent, while for longer wavelengths ($\bar{k}_\perp < 1, k_\perp \leq k_\parallel$), their electromagnetic character becomes prominent. This creates interesting space weather situations. For example, as lightning-generated whistlers propagate away from the Earth in the spatially varying density and magnetic field of the near-Earth environment, their wavelength must become shorter to remain consistent with the dispersion relation. This converts them into electrostatic lower hybrid waves at the lower hybrid surface where the wave frequency is equal to the local lower

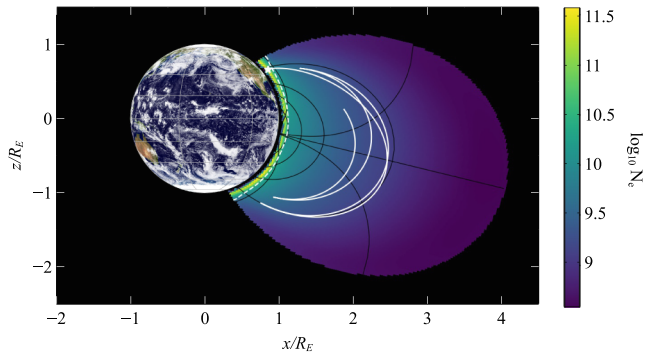

Figure 4. Result from a ray-tracing simulation of the propagation of whistler waves into the magnetosphere. The color background shows the electron density, as computed by the code SAMI2. The dashed curve shows the location where the ionospheric oxygen plasma gives way to the magnetospheric hydrogen plasma. The white curve shows the trajectory that the whistler wave takes through the magnetosphere, nearly following the field lines between the northern to southern hemispheres and reflecting at the lower hybrid cutoff when it nears the ionosphere (Earth Image Credit: NASA Goddard Space Flight Center. https://visibleearth.nasa.gov/view.php?id=57735).

hybrid frequency (Edgar, 1976). Electrostatic waves dissipate to produce plasma heating locally as opposed to spreading the energy over a larger volume and so create a different electromagnetic environment. This conversion is a linear process where the frequency remains unchanged.

More interestingly, however, for large enough amplitude, the lower hybrid waves generate electromagnetic whistler or magnetosonic waves through induced nonlinear scattering (Ganguli et al., 2010). This scattering process has been observed in the laboratory (Tejero et al., 2015, 2016) and is a fundamental process in weak turbulence. The rate at which lower hybrid waves (subscript LH) scatter into whistlers (subscript W) in the ionosphere is given by (Ganguli et al., 2015)

$$\gamma_{NL} \sim \frac{\omega_{pe}^2 \bar{k}_W^2}{\omega_{k_W}(1+\bar{k}_W^2)} \sum_{k_{LH}} \frac{(\mathbf{k}_{LH} \times \mathbf{k}_W)_\parallel^2}{k_{LH\perp}^2 k_{W\perp}^2} \frac{\bar{k}_{LH}^2}{1+\bar{k}_{LH}^2} \frac{\pi\zeta \mathrm{Im}(Z(\zeta))}{\left(1+\zeta_{c_s}^2\right)^2} \frac{|E_{k_{LH}}|^2}{4\pi n T_e}, \quad (3)$$

where T_e is the electron temperature, $E_{k_{LH}}$ is the lower hybrid wave electric field, $n = n_i = n_e$ is the density, $\zeta = (\omega_{k_{LH}} - \omega_{k_W})/(v_{te}|k_{LH\parallel} - k_{W\parallel}|)$, $\zeta_{c_s} = (\omega_{k_{LH}} - \omega_{k_W})/(c_s|\mathbf{k}_{LH} - \mathbf{k}_W|)$, $v_{te} = \sqrt{2T_e/m_e}$ is the electron thermal speed, $c_s = \sqrt{2T_e/m_i}$ is the sound speed, and $Z(\zeta) = \pi^{-1/2}\int_{-\infty}^{\infty} dt \exp(t^{-2})/(t-\zeta)$ is the plasma dispersion function. For the parameters of the SMART experiment, the order of magnitude of the nonlinear rate is $\gamma_{NL} \sim 10^7 (W_{LH}/nT_e)/s$, where $W_k \equiv |\mathbf{B}_k|^2/8\pi + (1+\omega_{pe}^2/\Omega_e^2)(|\mathbf{E}_k|^2/8\pi)$ is the wave energy density.

From equation (3) it can be seen that induced wave-particle scattering is a 3D kinetic phenomenon and that the scattering rate is large for large $\bar{k}_{LH}$, 90-degree azimuthal scattering, and large wave amplitude (i.e., large W/nT). The necessary condition for induced scattering is resonance between the beat wave phase speed and the particle thermal speed. In each scattering, the wave frequency decreases slightly, and the balance of wave energy is dissipated as plasma heating. The momentum conservation in this case involves the canonical momentum of magnetized electrons or ions, $(m\mathbf{v}_\perp + e\mathbf{A}/c)$, which includes the external magnetic field through the vector potential, $\mathbf{A}$. The external magnetic field can absorb wave momentum to facilitate large changes in scattered wave vectors, resulting in a significant change in the propagation angle. Consequently, induced scattering can lead to nonlinear conversion of electrostatic lower hybrid waves into electromagnetic whistler or magnetosonic waves, which can result in nonlocal energy flow.

As a consequence of induced scattering of the lower hybrid waves into electromagnetic whistlers with large group velocity, the turbulence energy can propagate away from the source region at the rate of

$$\gamma_p = \frac{1}{L}\frac{\partial\omega}{\partial k}, \quad (4)$$

where L is the source region dimension. For the parameters of the SMART experiment, this rate is $\gamma_p \sim 6\times 10^2/s$ (Ganguli et al., 2015). Figure 4 demonstrates the geographical spread of energy out of the source region into the realistic near-Earth space plasma environment obtained by a ray-tracing model. In order to obtain a realistic estimate of the dynamics of the whistler waves, the magnetospheric plasma state was computed using the code SAMI2 (Huba et al., 2000). The geophysical parameters used in the simulation are for quiet time, low solar activity conditions: F10.7 = 90, F10.7A = 90, and Ap = 4. The release occurs in the ionosphere near Wallops Island, VA: latitude 37° , longitude 285$^+$, and altitude 600 km. The day-of-year is 263 (mid-September), and the release time is 05:41 LT (i.e., pre-dawn).

The plasma parameters from this calculation were then used in the cold plasma dispersion function (Stix, 1992), and the ray equations were solved. Figure 4 shows both the trajectory of the ray and the plasma density from SAMI2. This ray was initialized at 550 km altitude and 37.8° latitude to match the parameters of the SMART experiment. The frequency was taken to be 5% higher than the local value of the lower hybrid frequency, and the wavevector had a small perpendicular component ($k_\perp/k_\parallel = 17.6\%$). As is typical for waves of this type, the ray first propagates nearly along the magnetic field lines high into the magnetosphere. It then bends back toward the Earth in the southern hemisphere but reflects as it approaches the lower hybrid cutoff. The process begins again, with the ray traveling back outward along the field lines and reflecting in

the northern hemisphere. This process repeats itself, with each bounce at lower peak altitude but larger k as the ray propagates away from the source region and into the magnetosphere.

This ability of the turbulence to convert from electrostatic to electromagnetic character and transport the energy out of the source region can be a major factor in determining the final plasma state in both laboratory and space plasmas. The significance of this process had not been realized before. It is particularly significant in space, where it can be harnessed to deliver energy to a remote location of interest. This provides a possible way to influence the space weather without the difficulties of limited power and plasma coupling that are typical for transmission of electromagnetic waves directly from an antenna.

There can be some loss of energy in the ionosphere due to dissipation, primarily through electron-ion collisional heating, which occurs at the rate (Crabtree et al., 2012)

$$\gamma_{ei} = -\frac{\nu_{ei}}{2}\frac{2\bar{k}_{\parallel}^2 + \bar{k}_{\perp}^2}{1+\bar{k}_{\perp}^2}, \tag{5}$$

where $\nu_{ei} = 3\times10^{-5} n_e T_e^{-3/2}$. The heating, however, is self-limiting since the electron-ion collision frequency is inversely proportional to the electron temperature. For the parameters of the SMART experiment, the order of magnitude rate is $\gamma_{ei} \sim (10-50)/s$ (Ganguli et al., 2015). In addition, the tail of the ion velocity distribution may resonate with the lower hybrid waves leading to the possibility of some energy loss through ion heating, which occurs at the rate $\gamma_{ih} \propto (\omega/kv_i)\exp(-(\omega/kv_i)^2)$. The wave phase speed $\omega/k \sim V_0 \sim$ 10 km/s (Mithaiwala et al., 2010) and the oxygen ion thermal speed $v_i \sim 1$ km/s. Since $\omega/kv_i \sim 10$ in the experiment the energy loss by ion heating will be negligible.

3.1. Hierarchy of Time Scales and Consequences on Energy Flux

For the parameters of interest to the SMART experiment, there is a hierarchy of time scales, $\gamma_{NL} > \gamma_r > \gamma_p > \gamma_{ei} > \gamma_{ih}$, in the interlinked physical processes of the weak turbulence triggered by the injection of the neutral Ba beam. This hierarchy governs the plasma dynamics that follows the onset of turbulence. There is a huge span in both the temporal and spatial scales associated with these processes. For example, the ionization time scale is 30 s while the lower hybrid wave grows over milliseconds. The lower hybrid wavelength is meters while the wavelength of the scattered whistlers is kilometers. The volume of the source region is about 10^{20} cm^3 in the ionosphere in a mostly oxygen plasma, while the energy spreads over a volume of 10^{26} cm^3 in the magnetosphere in a mostly hydrogen plasma and travels there through an inhomogeneous background of multi-species plasma embedded in dipolar magnetic field. Electromagnetic 3D PIC simulations are necessary to allow for the kinetic linear and nonlinear wave-particle interactions, which are critical. These interactions are localized over small regions in space while they cause energy flow over many thousands of kilometers. A single end-to-end PIC simulation of the evolution spread over such an enormous volume and including dynamic processes with multiple spatiotemporal scales in an inhomogeneous background is not feasible. Approximations that must be made to accommodate the diversity in scales (Winske & Daughton, 2012, 2015) make the results of the simulations unrealistic and hence inapplicable to the experiment (Ganguli et al., 2015; Rudakov et al., 2012). Hence, to understand the turbulence dynamics, we use wave kinetic analysis.

3.2. Wave Kinetic Analysis of the Plasma Dynamics

The wave kinetic equation that includes the interlinked physical processes with their characteristic time scales relevant to the SMART experiment is (Crabtree et al., 2012; Ganguli et al., 2012)

$$\frac{\partial W_k}{\partial t} = 2\gamma_r W_k - 2\gamma_d W_k - \gamma_{NL}(W_{k'})W_k - \gamma_p W_k, \tag{6}$$

where γ_d is the net (Landau and collisional) linear damping rate. The classical quasi-linear approach includes only the linear time scale that is represented by the first two terms in the right-hand side of equation (6). The third term represents the nonlinear processes, and the fourth term represents the radiation of energy out of the source region. The left-hand side represents the rate of net change in wave energy density in the source region as the turbulence evolves. At steady state a balance is achieved between the sources and sinks of wave energy consistent with their characteristic time scales. This balance will determine the realistic saturation time and the saturated wave amplitude along with the particle distribution, which collectively define the plasma state.

The scattered waves may be whistler waves, magnetosonic waves, or secondary lower hybrid waves. For the SMART parameters, the nonlinear scattering rate exceeds the linear damping rates, that is, $\gamma_{NL} > \gamma_{ei} > \gamma_{ih}$. Therefore, after birth the short wavelength electrostatic lower hybrid waves scatter into electromagnetic whistler or magnetosonic waves as well as to secondary lower hybrid waves before they can be significantly dissipated. In addition, both ion Landau and electron-ion collisional damping rates are smaller than the whistler propagation rate, that is, $\gamma_p > \gamma_{ei} > \gamma_{ih}$. Therefore, the scattered electromagnetic waves will exit the turbulent region in the ionosphere immediately and never return to it as illustrated in Figure 4. The scattered lower hybrid waves will continue to scatter a few more times until they become sufficiently electromagnetic to exit the source region. Since the dissipation in the source region is minimal, to leading order a steady state develops between the generation and propagation of whistler waves, and this physics is given by

$$\frac{dW_W}{dt} \approx -\gamma_p W_W + \gamma_{NL}(W_{LH})W_W = -10^2 W_W + 10^6 \frac{W_{LH}}{n_e T_e} W_W = 0. \tag{7}$$

Inserting the order of magnitude values of propagation and nonlinear scattering rates discussed earlier into equation (7), we see that at steady state the saturated value of the lower hybrid waves $W_{LH} \sim 10^{-4} n_e T_e$. Nonlinear Landau damping of lower hybrid waves, that is, the induced scattering process, will result in some energy loss before the waves become sufficiently electromagnetic and radiate out of the source region. This physics is given by

$$\frac{dW_{LH}}{dt} \approx \gamma_{LH} W_{LH} - \gamma_{NL}(W_{LH})W_{LH} - \gamma_{NL}(W_{LH})W_W, \tag{8}$$

$$\approx 10^3 W_{LH} - 10^7 \Delta\omega_k \frac{d}{d\omega_k} \frac{W_{LH}^2}{n_e T_e} - 10^6 \frac{W_{LH}}{n_e T_e} W_W = 0. \tag{9}$$

In equation (9) $\Delta\omega_k = \omega_{LH} - \omega_{W/MS}$ is the frequency reduction due to successive scatterings toward the formation of whistler or magnetosonic wave from a ring generated lower hybrid wave. The wave energy lost to the nonlinear Landau damping increases the electron temperature at the rate $n_e dT_e/dt \sim \gamma_{NL} W_{LH} \Delta\omega_k/\omega_{LH}$, which reduces the electron-ion collisional damping.

Equation (6) leads to important conclusions regarding the resulting turbulence. First, in the classical quasi-linear picture, most of the energy extracted from the beam ultimately returns to it, albeit as thermal energy, making $W_{beam}/W_{LH}^s \sim 1$, where W_{LH}^s and $W_{beam}(\equiv n_{Ba+} m_{Ba} \Delta V_{Ba+}^2/2)$ are the saturated lower hybrid wave energy density and the energy density extracted from the ring beam. In weak turbulence, however, most of the energy extracted from the beam goes to nonlinear processes or radiates away from the source region, and only a fraction can return to the beam. This makes the saturation time, $\tau_s \approx (1/\gamma_{LH})(W_{beam}/W_{LH}^s)$, much longer than in the quasi-linear limit since $W_{beam}/W_{LH}^s \gg 1$. Also, this makes the saturation amplitude of the lower hybrid waves smaller in weak turbulence than expected from the quasi-linear picture. Thus, in situ observation of low amplitude waves does not necessarily imply the absence of nonlinear effects. Second, this implies that 3D electromagnetic simulations of this process will have to be run for very long times (a time much longer than the time it takes the wave amplitude to saturate) to get a reasonable assessment of the conversion efficiency. Third, equations (7)–(9) imply that to lowest order a steady state is reached between the growth of wave energy through the generation of the lower hybrid waves and the loss through the propagation of the whistlers out of the source region, representing energy redistribution over a macroscopic scale. This is a significant result indicating that turbulence localized in space can act as an efficient antenna and broadcast large amounts of energy to affect the global space weather.

4. Discussion

The SMART experiment will inject approximately 1.5 kg of barium atoms at about 10 km/s, which implies initial energy injection of $\sim$ 37 MJ into the ionosphere at the start of the process. Simulations show that between 5% and 10% of the beam energy will be converted into the lower hybrid waves (Ganguli et al., 2015; Scales et al., 2012), which will ultimately be converted into whistler or magnetosonic waves and radiate out of the source region since the dissipation is negligible. A conservative assumption of only 5% extraction would imply that the turbulence energy in the source region is $\sim$ 1.8 MJ spread over a volume of 10^{20} cm^3 making the energy density $\sim 10^{-14}$ J/cm^3. This makes $W/n_e T_e \sim \mathcal{O}(1)$ large in the source region and ensures nonlinear scattering of these waves into whistlers or magnetosonic waves. These waves radiate into the

magnetosphere and expand over a volume of $\sim 10^{26}$ cm^3 (Crabtree et al., 2012). As a result, the energy density of the whistlers observed in the magnetosphere will be $\sim 10^{-20}$ J/cm^3 corresponding to an amplitude of $\sim$ 200 pT, which is similar in magnitude to strong lightning-generated whistlers that are routinely observed in the magnetosphere. Hence, the SMART-generated whistlers will be sufficiently intense for detection in the magnetosphere. In the magnetosphere $T_e \sim 0.75$ eV and $n_e \sim 3 \times 10^3$ cm^{-3}, making $W/n_eT_e = 5 \times 10^{-5}$, which determines the subsequent whistler dynamics in the magnetosphere.

4.1. Formation of a Resonant Cavity

A 3D ray-tracing model incorporating the effects of nonlinear scattering (Crabtree et al., 2012) was used to analyze the whistler propagation in the magnetosphere. During the transit from the ionosphere, the SMART-generated whistlers become increasingly electrostatic in the magnetosphere, converting into electrostatic lower hybrid-like waves. Without nonlinear scattering the wave energy dissipates. This is the same process that occurs with lightning-generated whistlers. At a certain altitude range they may come into cyclotron resonance with trapped electrons and precipitate them through pitch angle scattering (Ganguli et al., 2012). As discussed earlier, increasing wave vector increases the induced scattering rate, which scales as $\bar{k}^6$ in the magnetosphere (Crabtree et al., 2012) faster than the dissipation rate that scales as $\bar{k}^2$. Consequently, the wave will scatter before it is damped, albeit with some loss of energy. Since scattering with 90-degree azimuthal angle is more likely, the scattered wave follows nearly the same route to return toward the ionosphere (Crabtree et al., 2012). As the density increases toward the ionosphere, the whistlers are reflected back toward the magnetosphere. Depending on the albedo, some energy may be lost at reflection, but the reflected wave will continue to the lower hybrid surface and repeat the process all over again if the amplitude is sufficiently large to tolerate the loss. This will create a resonant cavity in which the whistlers traverse between the ionosphere and the lower hybrid surface and pitch angle scatter the trapped electrons multiple times (Crabtree et al., 2012) instead of dissipating at the lower hybrid surface, as would be the case without nonlinear scattering.

Repeated nonlinear scattering within the cavity keeps the average wave-normal angle small, which promotes efficient pitch angle scattering and hence shorter lifetime for the trapped electrons. The trapped electrons form an anisotropic loss cone distribution in which the loss cone is always empty. Hence, at each pitch angle scattering, the wave amplifies due to the loss cone instability (Ganguli et al., 2012; Kennel & Petschek, 1966). If the net gain is larger than the net loss, then the average whistler amplitude grows inside the cavity using the free energy from the trapped electron population, which in turn will enhance the pitch angle scattering rate and further amplify the whistlers. This feedback loop ceases when the flux of the trapped population drops below the threshold of the loss cone instability (Kennel & Petschek, 1966), but in the process, there is a significant reduction of the trapped population. Since satellite lifetime is inversely proportional to the trapped energetic electron population, this has a major practical implication.

With marginal energy $W/n_eT_e = 5 \times 10^{-5}$ in the magnetosphere, the SMART-generated whistlers are unlikely to sustain a cavity but may have enough energy for nonlinear scattering at the lower hybrid surface. To enhance the probability of scattering from the lower hybrid surface, the SMART experiment is designed with two successive injections of energy. The first one will increase the background value of W/nT so that the waves originating from the second injection will have an enhanced possibility for scattering. With the demonstration of the possibility to generate and broadcast whistlers into the radiation belts, the SMART experiment will establish a baseline case which can be scaled up to actively generate the resonant cavity. For example, instead of 1.5 kg if 150 kg of Ba is released at 10 km/s from a satellite in an elliptic orbit, then the wave amplitude in the magnetosphere would be $\sim$ 2 nT and the corresponding value of $W/n_eT_e = 5 \times 10^{-3}$. This is large enough to sustain the cavity (Crabtree et al., 2012) and subsequent amplification of the waves drawing out the free energy in the radiation belt loss cone distribution (Ganguli et al., 2012).

4.2. A Natural Example

A similar phenomenon may be sporadically occurring naturally in the radiation belts, as evidenced by the ability of some storm-enhanced radiation belts to quickly self-correct. The flux of relativistic electrons in the slot region in between the inner and outer radiation belts normally is $\sim 10^3$–10^4 electrons/cm^2/s (Fung et al., 2006; Schulz & Lanzerotti, 1974). During geomagnetic storms, the flux of trapped particles is pumped up in the slot. This is usually accompanied by injection of broadband waves as well. For example, during the Halloween storm, the energetic electron flux in this region was enhanced by 3–4 orders of magnitude (Baker et al., 2004, 2007). The trapped MeV electron flux level could get larger than $F \sim 10^6$ electrons/cm^2/s

(Brautigam et al., 2004). If the storm-injected wave amplitude is large enough, with at least a portion of the spectrum in cyclotron resonance with the trapped electrons, then large gain in amplitude of the waves is possible in the resonant cavity that will be formed. Strong electron precipitation along with wave amplification in the resonant cavity will ensue, leading to depletion of the trapped population.

Since the fraction of energy extraction is proportional to $\omega/(\Omega_e/\gamma_R)$ (Kennel & Petschek, 1966), the energy density of the resonant relativistic-trapped electrons that is potentially available for wave amplification is $(\omega\gamma_R/\Omega_e)n_R m\gamma_R c^2$, where n_R and γ_R are the cyclotron-resonant electron density and the relativistic Lorentz factor (Ganguli et al., 2012). This is typically much larger than the wave energy density in the magnetospheric cavity that is injected by the storm. Thus, even if just a small fraction of the available energy is initially extracted into the whistlers, an avalanche of energy will follow through multi-pass gain as described above. This will enhance the turbulence level resulting in rapid precipitation of the trapped electron population. This may explain why some storm-enhanced radiation belts that are accompanied with large amplitude waves in the right spectrum can quickly return to the normal background level. The rate at which an individual storm event is restored back to its normal background condition depends on the storm-related parameters such as wave amplitude and bandwidth, anisotropy, injection time, ans trapped flux level. Hence, it is different for different storms. A statistical analysis of data will be necessary to firmly establish this possibility.

5. Conclusion

We discussed the physics foundation for the upcoming in situ SMART experiment designed to study the properties of the evolution of turbulence in unbounded space plasmas and its consequences that cannot be accurately reproduced in laboratory. Besides elucidating the basic science issues, the experiment will also establish the ability to trigger weak turbulence on demand in the near-Earth space plasma for research or applications. The experiment will allow the study of the dual nature of the turbulence, that is, the interchangeability between electrostatic and electromagnetic character and its nonlocal consequences in the realistic environment. This property could potentially be used as a radiation source to generate and emit electromagnetic waves that will propagate out of the source region to affect the plasma condition at a remote location. In the process, the experiment will also show how energy is distributed from short to long wavelengths and spread over a large geographical volume in unbounded magnetized plasma that cannot be done in laboratory.

The energy input in the SMART experiment is through the kinetic energy that will be imparted to 1.5 kg of Ba atoms by shaped charge detonation (Ganguli et al., 2015; Koons & Pongratz, 1981). Subsequently, the Ba kinetic energy is converted into the electromagnetic energy through the formation of the unstable ion ring distribution in velocity. This will allow approximately 1.8 MJ of electromagnetic energy to be radiated into the magnetosphere. However, in a scaled-up experiment large amounts (150–200 kg) of Ba vapor can be introduced in the ionosphere at 10 km/s to yield approximately 0.5–1 GJ of electromagnetic energy, which may be further amplified in the resonant cavity that will be formed. The necessary kinetic energy (approximately 10 GJ) in this case can be obtained by using gravity to accelerate the Ba atoms by releasing them from a satellite in an elliptic orbit. For example, a satellite falling in gravity from an apogee of 30,000 km to perigee of 600 km can acquire a speed of around 10 km/s at the perigee. The free energy contained in the resulting plasma can be drawn directly and efficiently within minutes from the orbital kinetic energy which is greater and faster by many orders of magnitude than the energy that could conceivably be supplied to waves by any electrically driven antenna in space (Inan et al., 2003). Thus, using gravity, it is possible to unleash large amounts of energy and power rapidly via plasma turbulence to affect the near-Earth space environment over a macroscopic volume.

Acknowledgments
This work was supported by Naval Research Laboratory (NRL) Base Program and by Defense Advanced Research Projects Agency (DARPA). Data available at https://doi.org/10.7910/DVN/VRQWBC.

References

Alexandrova, O., Saur, J., Lacombe, C., Mangeney, A., Mitchell, J., Schwartz, S. J., & Robert, P. (2009). Universality of solar-wind turbulent spectrum from mhd to electron scales. *Physical Review Letters*, *103*, 165003. https://doi.org/10.1103/PhysRevLett.103.165003

Baker, D. N., Kanekal, S. G., Horne, R. B., Meredith, N. P., & Glauert, S. A. (2007). Low-altitude measurements of 2–6 MeV electron trapping lifetimes at 1.5≤ L≥ 2.5. *Geophysical Research Letters*, *34*, L20110. https://doi.org/10.1029/2007GL031007

Baker, D. N., Kanekal, S. G., Li, X., Monk, S. P., Goldstein, J., & Burch, J. L. (2004). An extreme distortion of the van allen belt arising from the 'Hallowe'en'solar storm in 2003. *Nature*, *432*(7019), 878–881.

Brautigam, D. H., Ray, K. P., Ginet, G. P., & Madden, D. (2004). Specification of the radiation belt slot region: Comparison of the NASA AE8 model with TSX5/CEASE data. *IEEE Transactions on Nuclear Science*, *51*(6), 3375–3380. https://doi.org/10.1109/TNS.2004.840024

Chatterjee, G., Schoeffler, K. M., Kumar Singh, P., Adak, A., Lad, A. D., Sengupta, S., et al. (2017). Magnetic turbulence in a table-top laser-plasma relevant to astrophysical scenarios. *Nature Communications*, *8*, 15970.

Crabtree, C., Rudakov, L., Ganguli, G., Mithaiwala, M., Galinsky, V., & Shevchenko, V. (2012). Weak turbulence in the magnetosphere: Formation of whistler wave cavity by nonlinear scattering. *Physics of Plasmas*, *19*(3), 032903. https://doi.org/10.1063/1.3692092

Edgar, B. C. (1976). The upper- and lower-frequency cutoffs of magnetospherically reflected whistlers. *Journal of Geophysical Research*, *81*(1), 205–211. https://doi.org/10.1029/JA081i001p00205

Fung, S. F., Shao, X., & Tan, L. C. (2006). Long-term variations of the electron slot region and global radiation belt structure. *Geophysical Research Letters*, *33*, L04105. https://doi.org/10.1029/2005GL024891

Ganguli, G., Crabtree, C., Mithaiwala, M., Rudakov, L., & Scales, W. (2015). Evolution of lower hybrid turbulence in the ionosphere. *Physics of Plasmas*, *22*(11), 112904. https://doi.org/10.1063/1.4936281

Ganguli, G., Rudakov, L., Crabtree, C., & Mithaiwala, M. (2012). Multi-pass whistler gain in a magnetospheric cavity due to induced nonlinear scattering. *Geophysical Research Letters*, *39*, L16105. https://doi.org/10.1029/2012GL052942

Ganguli, G., Rudakov, L., Scales, W., Wang, J., & Mithaiwala, M. (2010). Three dimensional character of whistler turbulence. *Physics of Plasmas*, *17*(5), 052310. https://doi.org/10.1063/1.3420245

Huba, J. D., Joyce, G., & Fedder, J. A. (2000). Sami2 is another model of the ionosphere (SAMI2): A new low-latitude ionosphere model. *Journal of Geophysical Research*, *105*(A10), 23,035–23,053. https://doi.org/10.1029/2000JA000035

Inan, U. S., Bell, T. F., Bortnik, J., & Albert, J. M. (2003). Controlled precipitation of radiation belt electrons. *Journal of Geophysical Research: Space Physics*, *108*(A5), 1186. https://doi.org/10.1029/2002JA009580

Kennel, C. F., & Petschek, H. E. (1966). Limit on stably trapped particle fluxes. *Journal of Geophysical Research*, *71*(1), 1–28. https://doi.org/10.1029/JZ071i001p00001

Kolmogorov, A. N. (1941). The local structure of turbulence in incompressible viscous fluid for very large reynolds numbers. *Doklady Akademii Nauk SSSR*, *30*, 301–304.

Koons, H. C., & Pongratz, . B. (1981). Electric fields and plasma waves resulting from a barium injection experiment. *Journal of Geophysical Research*, *86*(A3), 1437–1446. https://doi.org/10.1029/JA086iA03p01437

Mithaiwala, M., Rudakov, L., & Ganguli, G. (2010). Stability of an ion-ring distribution in a multi-ion component plasma. *Physics of Plasmas*, *17*(4), 042113. https://doi.org/10.1063/1.3372842

Reeves, G. D., McAdams, K. L., Friedel, R. H. W., & O'Brien, T. P. (2003). Acceleration and loss of relativistic electrons during geomagnetic storms. *Geophysical Research Letters*, *30*(10), 1529. https://doi.org/10.1029/2002GL016513

Rudakov, L., Crabtree, C., Ganguli, G., & Mithaiwala, M. (2012). Quasilinear evolution of plasma distribution functions and consequences on wave spectrum and perpendicular ion heating in the turbulent solar wind. *Physics of Plasmas*, *19*(4), 042704. https://doi.org/10.1063/1.3698407

Rudakov, L., Crabtree, C., Mithaiwala, M., & Ganguli, G. (2012). Analysis of winske-daughton 3D electromagnetic particle simulation of ion ring generated lower hybrid turbulence.

Rudakov, L., Mithaiwala, M., Ganguli, G., & Crabtree, C. (2011). Linear and nonlinear landau resonance of kinetic alfvn waves: Consequences for electron distribution and wave spectrum in the solar wind. *Physics of Plasmas*, *18*(1), 012307. https://doi.org/10.1063/1.3532819

Scales, W. A., Ganguli, G., Rudakov, L., & Mithaiwala, M. (2012). Model for nonlinear evolution of localized ion ring beam in magnetoplasma. *Physics of Plasmas*, *19*(6), 062902. https://doi.org/10.1063/1.4729330

Schulz, M., & Lanzerotti, L. J. (1974). *Particle Diffusion in the Radiation Belts*. Verlag: Springer.

Sorriso-Valvo, L., Marino, R., Carbone, V., Noullez, A., Lepreti, F., Veltri, P., et al. (2007). Observation of inertial energy cascade in interplanetary space plasma. *Physical review letters*, *99*, 115001. https://doi.org/10.1103/PHYSREVLETT.99.115001

Stix, T. H. (1992). *Waves in Plasmas*. New York: American Institute of Physics.

Tejero, E. M., Crabtree, C., Blackwell, D. D., Amatucci, W. E., Ganguli, G., & Rudakov, L. (2016). Experimental characterization of nonlinear processes of whistler branch waves. *Physics of Plasmas*, *23*(5), 055707. https://doi.org/10.1063/1.4946020

Tejero, E. M., Crabtree, C., Blackwell, D. D., Amatucci, W. E., Mithaiwala, M., Ganguli, G., & Rudakov, L. (2015). Nonlinear generation of electromagnetic waves through induced scattering by thermal plasma. *Scientific Reports*, *5*, 17852. https://doi.org/10.1038/srep17852

Van Allen, J. A., McIlwain, C. E., & Ludwig, G. H. (1959). Radiation observations with satellite 1958. *Journal of Geophysical Research*, *64*(3), 271–286. https://doi.org/10.1029/JZ064i003p00271

Winske, D., & Daughton, W. (2012). Generation of lower hybrid and whistler waves by an ion velocity ring distribution. *Physics of Plasmas*, *19*(7), 072109. https://doi.org/10.1063/1.4736983

Winske, D., & Daughton, W. (2015). Influence of plasma beta on the generation of lower hybrid and whistler waves by an ion velocity ring distribution. *Physics of Plasmas*, *22*(2), 022102. https://doi.org/10.1063/1.4906889